Vacuum 163 (2019) 210–215

Contents lists available at ScienceDirect

Vacuum

journal homepage: www.elsevier.com/locate/vacuum

Anharmonic correlated Debye model for thermal disorder in iron-rich B2-FeAl intermetallic alloy

Nguyen Thi Hong[a,b], Ho Khac Hieu[c], Nguyen Ba Duc[d,*], Duong Dai Phuong[e], Nguyen Viet Tuyen[b], Doan Quoc Khoa[f,g,**]

[a] Hong Duc University, Thanhhoa, Viet Nam
[b] VNU University of Science, 334 Nguyen Trai, Thanh Xuan, Hanoi, Viet Nam
[c] Institute of Research and Development, Duy Tan University, 03 Quang Trung, Hai Chau, Danang, Viet Nam
[d] Tan Trao University, Tuyen Quang, Viet Nam
[e] Military College of Tank Armour Officer, Vinhphuc, Viet Nam
[f] Division of Computational Physics, Institute for Computational Science, Ton Duc Thang University, Ho Chi Minh City, Viet Nam
[g] Faculty of Electrical and Electronics Engineering, Ton Duc Thang University, Ho Chi Minh City, Viet Nam

ARTICLE INFO

Keywords:
Thermal disorder
Anharmonicity
FeAl
Debye model
EXAFS cumulants

ABSTRACT

The anharmonic correlated Debye model has been developed to investigate the thermal disorder in B2-type FeAl intermetallic alloy. We derive analytical expressions of the bond-stretching force constants, the Debye temperature and frequency, the atomic mean-square displacement and the first three extended X-ray absorption fine structure (EXAFS) cumulants. Numerical calculations of these thermodynamic quantities have been performed for B2-type Fe-40 at.%Al up to temperature 1300 K using the Morse potential whose parameters were derived within the Möbius lattice inversion scheme. Our research shows that the anharmonicity contributions of thermal lattice vibrations are important to the EXAFS cumulants at high temperature. The theoretical predictions are compared with available experimental data when possible to verify the developed anharmonic correlated Debye model.

1. Introduction

The iron-aluminide (FeAl) is one of intermetallic alloys attracted attention of material scientists due to many its advanced physical properties such as relatively high strength, corrosion resistance behavior, high-temperature oxidation and high melting temperature [1]. The melting temperature of FeAl systems is predicted about 1583 K [2]. These interesting properties of FeAl promise it for various industrial applications, for instance, gas turbines, automobile engine components, protective coating for materials, substitution of ferritic stainless steels at high temperatures [3,4]. The FeAl intermetallic system exhibits several order/disorder phase transitions such as B2-type and DO3-type at various temperatures and compositions. Up to now, a numerous efforts have been dedicated to deeply understand the phase stabilities [5], vibration properties [6,7], heat capacities and mechanical properties [8,9] of FeAl systems.

Nevertheless, to our best knowledge, there are a few of researches regarding to the temperature effects on physical properties of FeAl alloy, and there is almost a lack of study of the thermal disorder in FeAl intermetallic compound. Thermal disorder stretches atomic positions in crystals, leading to a Gaussian distribution of interatomic distances in harmonic approximation [10,11]. The extended X-ray absorption fine structure (EXAFS) is one of the most powerful methods for considering local structure [12] and thermal behavior of materials [13,14]. This effect in EXAFS has been frequently analyzed by means of cumulant expansion approach in which an EXAFS oscillation function χ(k) is given as the following [15].

$$\chi(k) = \frac{F(k)}{kR^2} e^{-2R/\lambda(k)} Im\left\{ e^{i\phi(k)} \exp\left[2ikR + \sum_n \frac{(2ik)^n}{n!} C_n \right] \right\}, \quad (1)$$

where k and λ are, respectively, the wave number and mean free path of emitted photoelectrons, $F(k)$ is the real atomic backscattering amplitude, $\phi(k)$ is net phase shift, $R = \langle r \rangle$ denotes the thermal average distance (with r is the instantaneous bond length between absorber and back-scatterer atoms), and $C_n (n = 1,2,3, ...)$ are the EXAFS cumulants. The first cumulant C_1 denotes the mean value describing the net thermal

* Corresponding author.
** Corresponding author. Division of Computational Physics, Institute for Computational Science, Ton Duc Thang University, Ho Chi Minh City, Viet Nam.
E-mail addresses: ducnb@daihoctantrao.edu.vn (N.B. Duc), doanquockhoa@tdtu.edu.vn (D.Q. Khoa).

https://doi.org/10.1016/j.vacuum.2019.02.023
Received 26 December 2018; Received in revised form 13 February 2019; Accepted 13 February 2019
Available online 16 February 2019
0042-207X/

expansion or thermal disorder; the second cumulant C_2 describes the variance of the distance distribution corresponding to the mean-square relative displacement (MSRD) $\langle \Delta u_{\parallel}^2 \rangle$ parallel to the bond between pair absorber-backscatterer atoms which influence sensitively the EXAFS amplitude through the Debye-Waller factor $W(k) = \exp(2C_2k^2)$ [14]; and the third cumulant C_3 characterizes the asymmetry of the distribution function and it devotes to the phase shift of EXAFS spectroscopy [16].

In this work, we present the investigation of the thermal disorder in B2-type FeAl intermetallic alloy based on EXAFS theory. This type of FeAl intermetallic alloy, having the CsCl structure, remains stable in its structure with aluminum composition range 35–50 at.%. For this CsCl structure, each atom (Fe and Al) is bonded to eight nearest-neighbor atoms. Main aim of the present study is to investigate the temperature effects on EXAFS cumulants and related thermodynamic quantities. The anharmonic correlated Debye model (ACDM) [17] will be developed to derive the interatomic effective potential, bond-streching force constants, parallel $\langle \Delta u_{\parallel}^2 \rangle$ and perpendicular $\langle \Delta u_{\perp}^2 \rangle$ MSRDs, and the first three EXAFS cumulants. We then perform numerical calculations for B2-type Fe-40 at.%Al up to temperature 1300 K using the pair interaction Morse potential whose parameters were derived within the Möbius lattice inversion scheme.

2. Principle of calculations

2.1. Interatomic potential

In the first part, we present the procedure so-called the Möbius lattice inversion scheme to derive the pair interatomic potential for numerically calculating the thermodynamic properties of CsCl structure FeAl. Based on the Möbius inversion in the number theory, Chen et al. proposed the lattice inversion method to obtain the pair interatomic potential from the cohesive energy curves [18–21]. In within this approach, the cohesive energy per atom of a crystal $E(r)$ can be expressed as the sum of the interatomic potentials $\varphi(r)$ by

$$E(r) = \frac{1}{2}\sum_{i\neq j}\varphi(r_{ij}) = \frac{1}{2}\sum_{k=1}^{\infty} z_k \varphi(\nu(k) r_1), \tag{2}$$

where r_1 is the atomic nearest neighbor distance, $\nu(k) = \nu_k$ denotes the ratio of the k-th neighbor distance (r_k) to the first-neighbor distance r_1 (then $\nu_k r_1 = r_k$), and z_k is the coordination number of k-th neighbor atoms which denotes the number of atoms in k-th coordination sphere.

The pair interatomic potential $\varphi(r)$ is then derived through the inverse operation as

$$\varphi(r) = 2\sum_{k=1}^{\infty} I(k) E(\nu(k) r_1), \tag{3}$$

where $I(n)$ is the Möbius inversion function depending on structure type.

In current research, the pair interaction potential $\varphi(r)$ between two intermediate atoms is assumed to be the Morse function as

$$\varphi(r) = D_0\{\exp[-2\alpha(r - r_0)] - 2\exp[-\alpha(r - r_0)]\}, \tag{4}$$

where r_0 is the nearest-neighbor distance in the equilibrium reference structure, D_0 is the dissociation energy and α describes the width of the pair potential. These potential parameters for B2-FeAl alloy are fitted within the Möbius lattice inversion scheme.

2.2. Anharmonic effective potential

In this part, the anharmonic correlated Debye model (ACDM) [17,22] is summarized and the application of this model for body-centered cubic (BCC) structure will be presented briefly. The ACDM was developed based on the correlated Debye model to determine the anharmonicity contributions to EXAFS cumulants. This model considers a local vibration picture that includes near-neighbor correlations between absorber and back-scatterer atoms and their nearest neighbors. These interactions are described by an anharmonic interatomic effective potential V_{eff} which can be expressed as a function of the thermal expansion $x = r - r_0$ due to the asymmetry of the potential (with r and r_0 being the instantaneous and equilibrium distance between absorber and back-scatterer atoms, respectively) along the bond direction as

$$V_{eff}(x) = \varphi(x) + \sum_{j\neq i}\varphi\left(\frac{\mu}{M_i} x \hat{R}_{AB}\hat{R}_{ij}\right); \quad \mu = \frac{M_A M_B}{M_A + M_B}$$

$$\approx \frac{1}{2}k_{eff}x^2 + k_3x^3 + k_4x^4 + \ldots$$

where the interaction between absorber and backscatterer atoms is described by the potential term $\varphi(x)$. The last term in the right-hand side of Eq. (5) presents the influence of the neighboring atoms to the oscillation of absorber and back-scatterer, where the sum i is over absorber ($i = A$) and back-scatterer ($i = B$), and the sum j is over all their nearest neighbors, excluding the absorber and back-scatterer themselves; M_A and M_B are, correspondingly, the masses of the absorber and back-scatterer atoms in the given system; k_{eff} is the effective bond-stretching force constant, and k_3 and k_4 are the cubic and quartic bond-stretching force constants caused by an asymmetry in the pair distribution function due to the contribution of anharmonicity, respectively.

Previously, the ACDM was developed for pure crystalline metals [17]. If we apply the ACDM for BCC crystal, there are 14 pair interactions between absorber and back-scatterer with their nearest neighbor atoms, except for the absorber and back-scatterer themselves. Then the anharmonic interatomic effective potential V_{eff} in Eq. (5) for BCC system is calculated by

$$V_{eff}(x) = \varphi(x) + 2\varphi\left(-\frac{x}{2}\right) + 6\varphi\left(-\frac{x}{6}\right) + 6\varphi\left(\frac{x}{6}\right). \tag{6}$$

Assuming that the interaction between atoms in the system is described by the Morse potential (4), making the expansion of this Morse function up to the fourth order of the deviation of instantaneous bond length $r - r_0$, we have

$$\varphi(x) \approx D_0\left(-1 + \alpha^2x^2 - \alpha^3x^3 + \frac{7}{12}\alpha^4x^4\right), \quad x = r - r_0. \tag{7}$$

Substituting Eq. (7) into Eq. (6) we obtain the anharmonic interatomic effective potential $V_{eff}(x)$ as

$$V_{eff}(x) \approx \frac{11}{6}D_0\alpha^2x^2 - \frac{3}{4}D_0\alpha^3x^3 + \frac{1715}{2592}D_0\alpha^4x^4. \tag{8}$$

And the force constants of BCC crystal are then derived in terms of Morse potential parameters as follows

$$k_{eff} = \frac{11}{3}D_0\alpha^2;\ k_3 = -\frac{3}{4}D_0\alpha^3;\ k_4 = \frac{1715}{2592}D_0\alpha^4. \tag{9}$$

2.3. ACMD for iron-rich B2-FeAl alloy

In order to investigate the thermal disorder in the iron-rich B2-type FeAl compound, we need to develop the ACDM for alloy. For this purpose, we denote the concentration of Fe and Al in the ordered FeAl system being C_{Fe} and C_{Al}, respectively ($1 \geq C_{Fe} \geq C_{Al} \geq 0$). The interatomic effective potential V_{eff} of FeAl alloy is contributed not only by Fe–Al pairs but also by Fe–Fe interactions. This is depicted schematically in Fig. 1. The increasing of Al content will reduce the number of Fe–Fe nearest-neighbor bonds. Then the effective potential V_{eff} can be approximately determined as

$$V_{eff} = 2C_{Al}V_{eff}^{FeAl} + (C_{Fe} - C_{Al})V_{eff}^{Fe}, \tag{10}$$

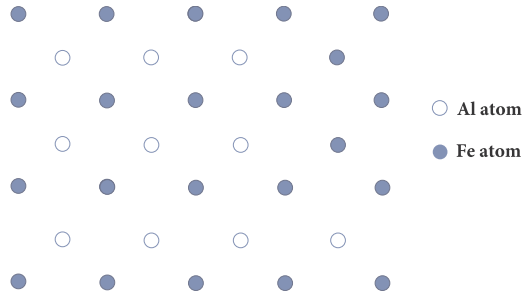

Fig. 1. Schematic representation of Fe–Al system in (110) plane.

where V_{eff}^{FeAl} and V_{eff}^{Fe} denote, respectively, the effective potential between *Fe* and *Al* atoms, and between *Fe* atoms.

From Eqs. (5) and (10), we derive the bond-stretching force constants k_{eff}, k_3 and k_4 of FeAl alloy as

$$k_{eff} = 2C_{Al}k_{eff}^{FeAl} + (C_{Fe} - C_{Al})k_{eff}^{Fe},$$

$$k_3 = 2C_{Al}k_3^{FeAl} + (C_{Fe} - C_{Al})k_3^{Fe},$$

$$k_4 = 2C_{Al}k_4^{FeAl} + (C_{Fe} - C_{Al})k_4^{Fe},$$

here k_{eff}^{Fe}, k_3^{Fe} and k_4^{Fe} have the forms similar to Eq. (9)

$$k_{eff}^{Fe} = \frac{11}{3}D_0^{Fe}(\alpha^{Fe})^2;\ k_3^{Fe} = -\frac{3}{4}D_0^{Fe}(\alpha^{Fe})^3;\ k_4^{Fe} = \frac{1715}{2592}D_0^{Fe}(\alpha^{Fe})^4, \tag{12}$$

and k_{eff}^{FeAl}, k_3^{FeAl} and k_4^{FeAl} are the force constants derived from the interatomic effective potential V_{eff}^{FeAl} between *Fe* and *Al* atoms.

$$k_{eff}^{FeAl} = \left[1 + \frac{5}{3}(\mu_{Fe}^2 + \mu_{Al}^2)\right]D_0^{FeAl}(\alpha^{FeAl})^2;$$

$$k_3^{FeAl} = -[1 - \mu_{Fe}^3 - \mu_{Al}^3)]D_0^{FeAl}(\alpha^{FeAl})^3;$$

$$k_4^{FeAl} = \left[\frac{7}{12} + \frac{203}{324}(\mu_{Fe}^4 + \mu_{Al}^4)\right]D_0^{FeAl}(\alpha^{FeAl})^4,$$

with

$$\mu_{Fe} = \frac{M_{Fe}}{M_{Fe} + M_{Al}}, \quad \mu_{Al} = \frac{M_{Al}}{M_{Fe} + M_{Al}}. \tag{14}$$

The Debye frequency and Debye temperature of alloy system are calculated, respectively, as the following [17].

$$\omega_D = 2\sqrt{\frac{k_{eff}}{m}} \quad ; \quad \theta_D = \frac{\hbar\omega_D}{k_B}, \tag{15}$$

where m is the average atomic mass which is determined as

$$m = 2C_{Al}m_{FeAl} + (C_{Fe} - C_{Al})m_{Fe}, \tag{16}$$

and $m_{FeAl} = (m_{Fe} + m_{Al})/2$.

The thermal disorder of atoms in materials can be described by the moments of atomic displacement so-called cumulants in EXAFS theory. The definition of EXAFS cumulants is based on the cumulant expansion approach [14,15]. The first three EXAFS cumulants of B2-FeAl alloy in ACDM [17] are then derived, respectively, as

$$C_1 = \langle r - r_0\rangle = \sigma_0^{(1)}\int_0^{\pi/a}\omega(q)\frac{1 + z(q)}{1 - z(q)}dq, \tag{17}$$

$$C_2 = \langle (r - r_0 - C_1)^2\rangle = \sigma_0^{(2)}\int_0^{\pi/a}\omega(q)\frac{1 + z(q)}{1 - z(q)}dq, \tag{18}$$

$$C_3 = \langle (r - r_0 - C_1)^3\rangle = \sigma_0^{(3)}\int_0^{\pi/a}dq_1\int_{-\pi/a}^{\pi/a-q_1}F(q_1, q_2)dq_2, \tag{19}$$

where

$$F(q_1, q_2) = \frac{\omega(q_1)\omega(q_2)\omega(q_1 + q_2)}{\omega(q_1) + \omega(q_2) + \omega(q_1 + q_2)}\times$$

$$\times\left\{1 + 6\frac{\omega(q_1) + \omega(q_2)}{\omega(q_1) + \omega(q_2) - \omega(q_1 + q_2)}\frac{z(q_1)z(q_2) - z(q_1 + q_2)}{[z(q_1) - 1][z(q_2) - 1][z(q_1 + q_2) - 1]}\right\},$$

and $\beta = 1/k_BT$ with k_B is the Boltzmann constant.

Here, the $\sigma_0^{(1)}$, $\sigma_0^{(2)}$, and $\sigma_0^{(3)}$ are, respectively, the zero-point contributions to the first, the second, and the third cumulants which have the forms as the following

$$\sigma_0^{(1)} = \frac{3\hbar a}{2\pi}\frac{2C_{Al}k_3^{FeAl} + (C_{Fe} - C_{Al})k_3^{Fe}}{[2C_{Al}k_{eff}^{FeAl} + (C_{Fe} - C_{Al})k_{eff}^{Fe}]^2}, \tag{21}$$

$$\sigma_0^{(2)} = \frac{\hbar a}{2\pi}\frac{1}{2C_{Al}k_{eff}^{FeAl} + (C_{Fe} - C_{Al})k_{eff}^{Fe}}, \tag{22}$$

$$\sigma_0^{(3)} = \frac{3\hbar^2a^2}{4\pi^2}\frac{2C_{Al}k_3^{FeAl} + (C_{Fe} - C_{Al})k_3^{Fe}}{[2C_{Al}k_{eff}^{FeAl} + (C_{Fe} - C_{Al})k_{eff}^{Fe}]^3}. \tag{23}$$

3. Numerical calculations and discussion

The expressions derived in the previous section are now applied to investigate the thermodynamic properties of the B2-type FeAl. Numerical calculations have been performed for B2-type FeAl with 40% Al. Using the quantum approximate method of Bozzolo-Ferrante-Smith, Grosso et al. showed that the melting temperature of B2-type Fe-40 at.%Al is about 1704 K [23]. The fitted parameters of Morse potential for B2-type FeAl within the Möbius lattice inversion scheme are shown in Table 1 [1].

Applying our developed ACDM model, the three force constants of B2-type Fe-40 at.%Al are derived as follows $k_{eff} = 2.4020$ eV/Å^2, $k_3 = -2.2353$ eV/Å^3 and $k_4 = 3.4431$ eV/Å^4. Using the effective bond-stretching force constant k_{eff}, we find out the Debye temperature and Debye frequency of B2-type FeAl, respectively, as 350 K and 4.58×10^{13} Hz. This value of Debye temperature is reasonable consistent with the one (385 ± 5) K derived from the intensity analysis of diffraction lines of Mössbauer spectroscopy [24]. The slight difference between Debye temperatures can be caused by the different techniques and different conditions which have been exploited to evaluate. The difference between our theoretical prediction and experimental measurement of Debye temperature is about 9%. The Debye temperature is one of the most important physical quantities derived in within view of the Debye model. For the crystal with N atoms, the Debye model assumes a homogeneous system with a constant speed of sound c and the linear dispersion relation $\omega = c.\ k$. The maximum phonon frequency ω_D is so-called the Debye frequency, and $\theta_D = \hbar\omega_D/k_B$ is the Debye temperature above which all modes begin to be excited and below which modes begin to be "frozen out" [25]. Hence, the Debye temperature could be exploited to estimate the high and low temperature regions for the thermodynamic properties of solids.

From the first shell interatomic distance of the FeAl system calculated by using the ACDM, we can approximate the thermal behavior of nearest-neighbor distance as $R(T) \approx R(0) + C_1$. And the lattice parameter of B2-FeAl is then derived by $a_h(T) = 2/\sqrt{(3)}$. In Fig. 2, we show the temperature-dependent lattice constant of B2-type Fe-40 at.%Al in the temperature range 0–1300 K. The solid line presents our results compared with those of experimental data (◆ symbols) measured by high-temperature X-ray diffractometry [8]. As it can be seen in Fig. 2 that the theoretical predictions in EXAFS theory are larger than those of experimental crystallographic measurements. This behavior is of

Table 1
The fitted parameters of Morse potential for B2-type FeAl [1].

$A - B$	D_0^{A-B} (Å)	α^{A-B} (eV)	r_0^{A-B} (Å^{-1})
Fe–Fe	0.346	2.562	2.507
Fe–Al	0.269	1.850	2.656

Table 2
The bond-stretching force constant k_{eff}, the Debye frequency ω_D and Debye temperature θ_D of B2-type Fe-40 at.%Al derived from developed ACDM.

Alloy	k_{eff} (eV/Å^2)	ω_D ($\times 10^{13}$ Hz)	θ_D (K)
Present theory	2.4020	4.58	350
Experiments	–	5.04[24]	385[24]

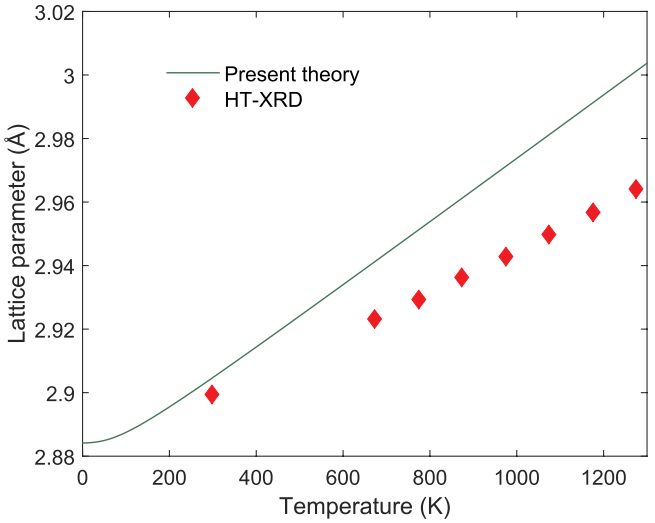

Fig. 2. Temperature-dependent lattice parameter of FeAl. Our calculations (solid lines) are presented in comparison to experimental high-temperature X-ray diffractometry (HT-XRD) measurements [8].

geometrical origin which has been pointed out by Fornasini et al. before [26]. The mismatch between theory and high-temperature X-ray diffractometry experiment is gradually prominent with temperature and the maximum difference is about 1–2% at 1300 K.

Fig. 3 reports the temperature effects on the second cumulant of FeAl system in our calculations. It should be noted that the second cumulant C_2 corresponds to the parallel atomic MSRD characterizing the EXAFS Debye-Waller factor that influences on the amplitude of EXAFS oscillations. This factor is susceptible to both the temperature-independent structural disorder (or static disorder caused by strain or alloying) and thermal disorder. The latter quantity represents thermal vibrations and provides information on the bond-stretching force constant between absorber-backscatterer pair corresponding to the dynamical properties of them. In the inset figure, the measurements of the changes of Debye-Waller factor C_2 relative to the lowest temperature value denoted by ΔC_2 (in Å^{-2}) for the first three-shell distances of FeAl metal are shown for comparison [6]. With regard to the above mentioned, the Debye-Waller factor in our calculations (the solid line) has been vertically adjusted downward. The temperature-independent shifting value $\sigma^2_{static} = 0.9 \times 10^{-3}$ Å^2 can be seen as a static disorder contribution to the second cumulant C_2. As observed in this figure that the good agreement between theoretical predictions and experimental measurements for the third-neighbor shell is found. Notwithstanding, the Debye-Waller factor increases rapidly with temperature, and above 150 K, the almost linear proportion to temperature of C_2 could be observed. The slope of C_2 at temperature beyond 150 K is $dC_2/dT = 3.50 \times 10^{-5}$ Å^2/K. The robust increasing of C_2 evidences the important contributions of thermal disorder at high temperature region.

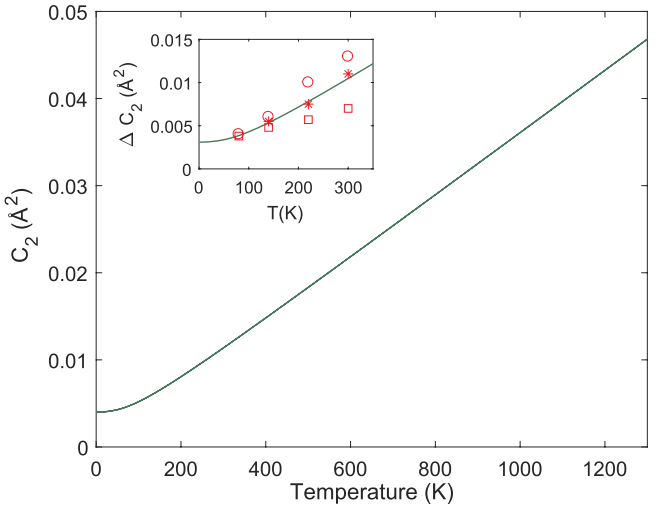

Fig. 3. Temperature-dependence of the second cumulant of FeAl. The experimental measurements of the changes of Debye-Waller factor ΔC_2 (in Å^{-2}) for the first three-shell distances of FeAl metal are shown for comparison [6].

Here it is worth mentioning that the difference between EXAFS and crystallographic thermal expansion (and also lattice parameter) could be used to deduce the information of the MSRD $\Delta u_\perp^2$ perpendicular to bond between absorber and back-scatterer atoms. The larger of average distance measured by EXAFS comparing to the crystallographic distance is of the geometrical origin and can be described by the following equation [26].

$$\langle r \rangle \simeq R_c + \langle \Delta u_\perp^2 \rangle / 2R_c, \tag{24}$$

where R_c is the crystallographic distance measured by Bragg diffraction experiment.

Using Eq. (24), we derive the perpendicular MSRD $\langle \Delta u_\perp^2 \rangle$ of a pair of absorber and back-scatterer atoms of current system. The temperature effects on the perpendicular MSRD $\langle \Delta u_\perp^2 \rangle$ and parallel MSRD $\langle \Delta u_\parallel^2 \rangle$ of B2-type Fe-40 at.%Al are shown in Fig. 4. As can be observed in this figure, the perpendicular MSRD $\langle \Delta u_\perp^2 \rangle$ are always larger than the corresponding values of the parallel MSRD. And the gap between perpendicular and parallel MSRD increases with the increasing of temperature. Usually, the difference between two quantities is summarized by the temperature-dependent ratio $\gamma = \langle \Delta u_\perp^2 \rangle / \langle \Delta u_\parallel^2 \rangle$. This ratio characterizes for the perpendicular to parallel anisotropy of relative vibrations of neighboring atoms [27]. For ideal Debye crystal, the ratio γ is equal to 2 [26], and for copper, the ratio $\gamma = 2.7$ is obtained by path-integral Monte-Carlo calculations [28]. In our work, the ratio γ of B2-type Fe-40 at.%Al is greater than 4.3 in the temperature range 0–1300 K. The difference between the ratio γ can be caused by the peculiar effect of the optical modes in non-Bravais crystals [26].

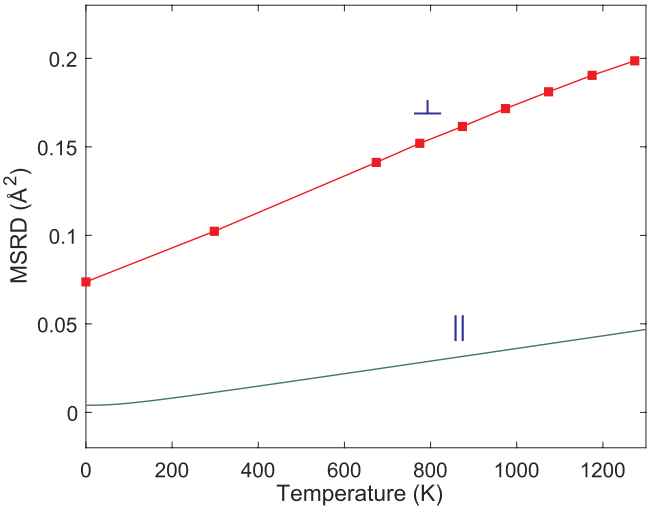

Fig. 4. Temperature-dependence of the parallel and perpendicular mean-square relative displacement (MSRD) of FeAl.

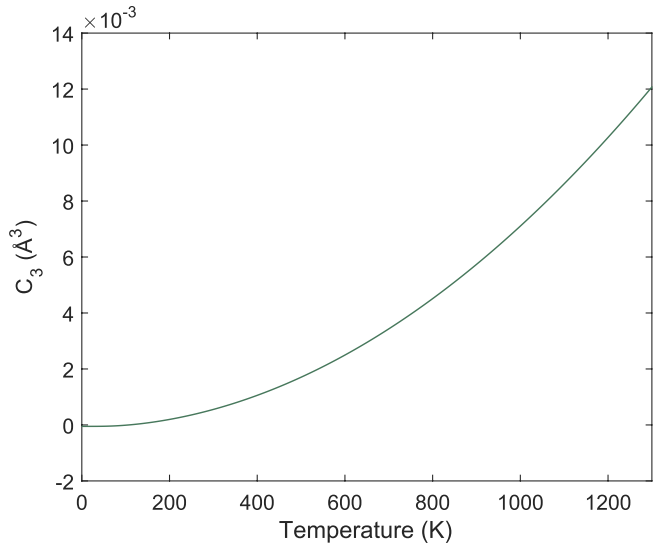

Fig. 5. Temperature-dependence of the third cumulant C_3 of FeAl.

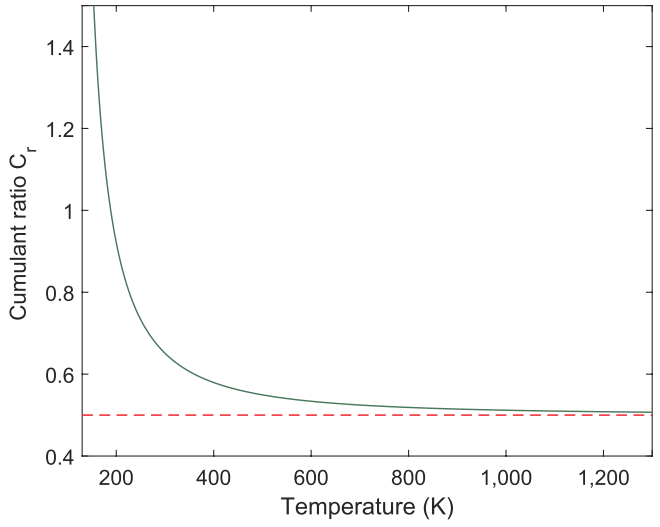

Fig. 6. Temperature dependence of cumulant ratio C_r of FeAl.

The temperature dependence of the asymmetry parameter C_3 obtained from the current developed ACDM up to 1300 K is shown in Fig. 5. Similarly to C_2, the third cumulant C_3 increases progressively with temperature. However, it almost follows the function T^2 at high temperature. The slope of C_3 curve in the temperature range 350–1300 K is about $dC_3/dT = 9.0 \times 10^{-6}$ Å^3/K. The rising of C_3 makes the deviation of the effective distribution function from a Gaussian approximation. Because there is no available experimental data, the comparison in this case has been neglected.

Furthermore, in the theory of EXAFS, one of the important quantity considered as a criterion for cumulant investigation is the cumulant ratio C_r which is defined as $C_r = C_1.\ C_2/C_3$ [29]. Previous work showed that the ratio C_r progressively tends to the constant value of 1/2 when temperature increases. Then we can use this ratio to evaluate the temperature threshold above which the classical limit is applicable. The temperature-dependent cumulant ratio C_r of intermetallic alloy FeAl calculated within the present ACDM scheme is presented in Fig. 6. As it can be observed from this figure, the threshold temperature is surmised about 900 K. It means that the classical region is beyond 900 K. Below temperature 900 K the classical calculations will be invalidity. Meanwhile, the quantum approach is suitable for various temperature, but it should diminish to the classical limit at temperature region of higher than 900 K. The current developed ACDM inherits all of the advantages of the classic ACDM. This means that the derived cumulants include the zero point vibration contributions (a quantum effects) at low temperature, and the anharmonicity contributions of thermal vibrations at high temperature.

Before making conclusions, it should be noted that the temperature dependence of EXAFS cumulants can be studied by means of various techniques such as Debye model [17,22], Einstein model [30] and path-integral effective-potential theory [31]. Computer simulation including density functional theory (DFT) calculations is also another approach. However, to our best knowledge, there is no DFT calculation that has been performed for FeAl systems as well. Furthermore, because of the existence of many of simulation tools, the choice of technique requires a good understanding of basic principles. More importantly, understanding of the basic principles could greatly improve the efficiency of a simulation program. Finally, another advantage of developed ACDM in comparison with DFT calculations is the apparent analytical expressions of EXAFS cumulants. These formulae allow us easily and quickly determine the EXAFS cumulants of FeAl systems with various temperature and concentration.

4. Conclusions

In this work, the thermal disorder in B2-FeAl alloy has been investigated basing on the developed anharmonic correlated Debye model. The Morse potential whose parameters were derived within the Möbius lattice inversion scheme has been exploited to numerically calculate the parallel and perpendicular mean-square relative displacement and first three EXAFS cumulants up to temperature 1300 K. Our research shows that the anharmonicity contributions of thermal lattice vibrations are important to the EXAFS cumulants at high temperature. The good and reasonable agreement of our calculated results with experiments denotes the efficiency of the developed model in the investigation of the temperature effects on other EXAFS parameters.

Acknowledgements

The authors would like to thank Prof. Nguyen Van Hung for useful comments and suggestions. This research is funded by the Vietnam National Foundation for Science and Technology Development (NAFOSTED) under grant number 103.01-2017.343.

Appendix A. Supplementary data

Supplementary data to this article can be found online at https://doi.org/10.1016/j.vacuum.2019.02.023.

References

[1] C.-H. Zhang, S. Huang, J. Shen, N.-X. Chen, Intermetallics 52 (2014) 86 ISSN 0966-9795 http://www.sciencedirect.com/science/article/pii/S0966979514001101.
[2] R. Nakamura, K. Takasawa, Y. Yamazaki, Y. Iijima, Intermetallics 10 (2002) 195 ISSN 0966-9795 http://www.sciencedirect.com/science/article/pii/S096697950100125X.
[3] C. Cazorla, S.G. MacLeod, D. Errandonea, K.A. Munro, M.I. McMahon, C. Popescu, J. Phys. Condens. Matter 28 (2016) 445401 https://doi.org/10.1088%2F0953-8984%2F28%2F44%2F445401.
[4] D. Smith, O.P.J. Joris, A. Sankaran, H.E. Weekes, D.J. Bull, T.J. Prior, D. Dye, D. Errandonea, J.E. Proctor, J. Phys. Condens. Matter 29 (2017) 155401 https://doi.org/10.1088%2F1361-648x%2Faa60b6.
[5] M.H. Jacobs, R. Schmid-Fetzer, Calphad 33 (2009) 170 ISSN 0364-5916, experimental and Computational investigation of intermetallic systems: A Special Issue Dedicated to Prof. Riccardo Ferro http://www.sciencedirect.com/science/article/pii/S0364591608000618.
[6] D. Brewe, D.M. Pease, J.I. Budnick, C.C. Law, Phys. Rev. B 56 (1997) 11449 https://link.aps.org/doi/10.1103/PhysRevB.56.11449.
[7] L. Shaojun, D. Suqing, M. Benkun, Phys. Rev. B 58 (1998) 9705 https://link.aps.org/doi/10.1103/PhysRevB.58.9705.
[8] M. Zhao, K. Yoshimi, K. Maruyama, K. Yubuta, Acta Mater. 64 (2014) 382 ISSN 1359-6454 http://www.sciencedirect.com/science/article/pii/S1359645413008148.

[9] T. Zienert, A. Leineweber, O. Fabrichnaya, J. Alloy. Comp. 725 (2017) 848 ISSN 0925-8388 http://www.sciencedirect.com/science/article/pii/S0925838817325768.
[10] G. Dalba, P. Fornasini, J. Synchrotron Radiat. 4 (1997) 243 https://doi.org/10.1107/S0909049597006900.
[11] A. Momozawa, R. Telle, Vacuum (2018), https://doi.org/10.1016/j.vacuum.2018.06.036 ISSN 0042-207X http://www.sciencedirect.com/science/article/pii/S0042207X17316627.
[12] F. Pan, D. Cao, Z. Wu, J. Liu, Y. An, Vacuum 139 (2017) 122 ISSN 0042-207X http://www.sciencedirect.com/science/article/pii/S0042207X1730026X.
[13] T.M. Willis, A.W. Pryor, Thermal Vibrations in Crystallography, Cambridge University Press, Cambridge, U.K, 1975.
[14] E.D. Crozier, J.J. Rehr, R. Ingalls, D.C. Koningsberger, R. Prins (Eds.), X-Ray Absorption: Principles, Applications, Techniques of EXAFS, SEXAFS and XANES, first ed., Wiley-Interscience, 0471875473, 1988, http://www.amazon.com/X-Ray-Absorption-Principles-Applications-Techniques/dp/0471875473.
[15] G. Bunker, Nucl. Instrum. Methods Phys. Res. 207 (1983) 437 ISSN 0167-5087 http://www.sciencedirect.com/science/article/pii/0167508783906555.
[16] G. Dalba, D. Diop, P. Fornasini, F. Rocca, J. Phys. Condens. Matter 6 (1994) 3599 http://stacks.iop.org/0953-8984/6/i=19/a=016.
[17] N.V. Hung, N.B. Trung, B. Kirchner, Phys. B Condens. Matter 405 (2010) 2519 ISSN 0921-4526 http://www.sciencedirect.com/science/article/pii/S0921452610002656.
[18] N.-x. Chen, Phys. Rev. Lett. 64 (1990) 1193 https://link.aps.org/doi/10.1103/PhysRevLett.64.1193.
[19] N.-X. Chen, Y. Chen, G. ying Li, Phys. Lett. 149 (1990) 357 ISSN 0375-9601 http://www.sciencedirect.com/science/article/pii/037596019090893S.
[20] S.-J. Liu, M. Li, N.-X. Chen, J. Phys. Condens. Matter 5 (1993) 4381 http://stacks.iop.org/0953-8984/5/i=26/a=010.
[21] N. xian Chen, M. Li, S. jun Liu, Phys. Lett. 195 (1994) 135 ISSN 0375-9601 http://www.sciencedirect.com/science/article/pii/0375960194900868.
[22] N.B. Duc, V.Q. Tho, N.V. Hung, D.Q. Khoa, H.K. Hieu, Vacuum 145 (2017) 272 ISSN 0042-207X http://www.sciencedirect.com/science/article/pii/S0042207X17307716.
[23] M. del Grosso, H. Mosca, G. Bozzolo, Intermetallics 18 (2010) 945 ISSN 0966-9795 http://www.sciencedirect.com/science/article/pii/S0966979510000245.
[24] S.H. Mahmood, M.A. Awawdeh, A.S. Saleh, J. Appl. Phys. 73 (1998) 5663 ISSN 0021-8979 https://doi.org/10.1063/1.353637.
[25] N.W. Ashcroft, N.D. Mermin, Solid State Physics, first ed., Cengage Learning, 1976, https://www.amazon.com/Solid-State-Physics-Neil-Ashcroft/dp/0030839939.
[26] P. Fornasini, S. a Beccara, G. Dalba, R. Grisenti, A. Sanson, M. Vaccari, F. Rocca, Phys. Rev. B 70 (2004) 174301 https://link.aps.org/doi/10.1103/PhysRevB.70.174301.
[27] P. Fornasini, R. Grisenti, J. Synchrotron Radiat. 22 (2015) 1242 https://doi.org/10.1107/S1600577515010759.
[28] S. a Beccara, G. Dalba, P. Fornasini, R. Grisenti, F. Pederiva, A. Sanson, D. Diop, F. Rocca, Phys. Rev. B 68 (2003) 140301 https://link.aps.org/doi/10.1103/PhysRevB.68.140301.
[29] N.V. Hung, J.J. Rehr, Phys. Rev. B 56 (1997) 43 http://link.aps.org/doi/10.1103/PhysRevB.56.43.
[30] A.I. Frenkel, J.J. Rehr, Phys. Rev. B 48 (1993) 585 http://link.aps.org/doi/10.1103/PhysRevB.48.585.
[31] T. Yokoyama, Phys. Rev. B 57 (1998) 3423 http://link.aps.org/doi/10.1103/PhysRevB.57.3423.